Comput. Methods Appl. Mech. Engrg. 197 (2008) 3378–3385

Contents lists available at ScienceDirect

Comput. Methods Appl. Mech. Engrg.

journal homepage: www.elsevier.com/locate/cma

Quantum dot–DNA interaction: Computational issues and preliminary insights on use of quantum dots as biosensors

S. Anandampillai [a], X. Zhang [a], P. Sharma [a,b,*], Gillian C. Lynch [c], M.A. Franchek [a,d], K.V. Larin [a,d,e]

[a] Department of Mechanical Engineering, University of Houston, Houston 77204, TX, USA
[b] Department of Physics, University of Houston, Houston 77204, TX, USA
[c] Department of Chemistry, University of Houston, Houston 77204, TX, USA
[d] Biomedical Engineering Program, University of Houston, Houston 77204, TX, USA
[e] Institute of Optics and Biophotonics, Saratov State University, Saratov, Russia

ARTICLE INFO

Article history:
Received 9 September 2007
Received in revised form 2 February 2008
Accepted 20 February 2008
Available online 7 March 2008

Keywords:
Quantum dots
DNA
Biomedical applications

ABSTRACT

In recent years, quantum dots have generated enormous interest from the life sciences community due to their (largely) untapped potential in biomedical applications; particularly in bio-labeling and sensing. While empirical work already exists on the use of quantum dots as bio-labels, their development as biosensors requires a thorough scientific understanding of their interactions with conjugated biomolecules that together 'sense' the molecule of interest. Some recent experiments have claimed a marked variation in the luminescence of cadmium selenide quantum dots conjugated to macromolecules linked to bacteria. The origin of this large shift in luminescence of the quantum dot (and thus by implication, the band gap) appears to be poorly understood. The knowledge of the exact nature of the interaction causing the 'shift' may hold the key to designing better biosensors. The objective of the present work is to address the aforementioned interaction and to that end, we have chosen a prototypical model consisting of a capped cadmium selenide quantum dot interacting with a DNA molecule. This problem is inherently multiscale due to the relatively large number of atoms, complex nature of the interactions involved in the quantum dot–DNA system and the disparate length scales present in the problem requiring a combination of methods ranging from approaches that utilize empirical molecular mechanics force fields on one hand and *ab initio* electronic structure (based on density functional theory) calculations on the other hand. We discuss several modeling issues that arise in the simulations of this complex problem and present some preliminary insights. Our initial results indicate a wavelength shift of roughly 19 nm in the spectrum of a 1.1 nm sized dot upon interaction with a typical DNA molecule. However, upon increase of quantum dot size, the shift decreases and thus suggests a re-examination of singular experimental data available in the literature. Our results, which are performed in vacuum rather than a solvent, may be considered as an upper-bound to the true interaction.

1. Introduction

When bulk semiconductors like cadmium selenide (CdSe) or Gallium Arsenide (GaAs) are shrunk in size to a few nanometers, their opto-electronic, mechanical and other physical properties alter dramatically when compared with corresponding bulk ones. These nanoparticles, or quantum dots, contain very few charge carriers and this so-called quantum confinement is largely responsible for their unusual optical and electronic properties. Although there are other interesting aspects of electronic behavior of three dimensionally confined quantum dots, the ability to tailor the electronic structure and hence optical response of quantum dots with minute changes in size is one that is most often emphasized.

Although of recent vintage, extensive literature has already appeared on the use of quantum dots as biological labels [27]. Correspondingly far fewer works have addressed their role as *sensors*. Semiconductor quantum dots (like zinc sulfide-capped CdSe) may be functionalized with a unique ligand–biomolecule pair to facilitate binding to a particular biological structure for use in ultrasensitive biological detection. The possibility of large scale applications of quantum dots in bio-sensing, fluorescent spectroscopy, separation and assaying techniques [2] has created the need for a better understanding of the conjugation process at the atomistic level. For better control over the 'design' of quantum dot-bioconjugates, an improved understanding of the interactions which leads to a stable conjugation is required. The wavelength shift is

* Corresponding author. Address: Department of Mechanical Engineering, University of Houston, Houston 77204, TX, USA.
E-mail address: psharma@uh.edu (P. Sharma).

0045-7825/$ - see front matter © 2008 Elsevier B.V. All rights reserved.
doi:10.1016/j.cma.2008.02.032

one such phenomenon that can be a favorable mechanism in biosensing if it can be achieved by conjugation with known ligands with a unique number set for each class of ligand molecules. The exact mechanisms for wavelength shifts in the spectrum of quantum dots are still not fully understood for the case when a quantum dot is conjugated to a DNA – bacteria complex or other macromolecules found in biological systems. Dwarakanath et al. [11] claim to have experimentally observed a 'blue shift' (~140 nm in one case) in the emission wavelength when a CdSe–ZnS quantum dot was conjugated to a DNA aptamer or an antibody that was bound to a bacterium. Similar shifts have been seen by other experimentalists with lower level wavelength changes [42,14]. Whether or not the large spectral shift observed is repeatable under different experimental conditions and can be explained by a unified theory is debatable. The present work aims to present a preliminary study based on computational physics and chemistry for such a system consisting of a capped CdSe quantum dot and a DNA molecule as a prototype system to understand the interactions that occur between quantum dots and biomolecules on an atomic level. Apart from physical insights we also discuss the computational challenges that we faced. We have limited our focus to understanding non-bonded interactions in the chosen system. Owing to the complexity of the nature of the interactions and the large number of atoms in the quantum dot–DNA system, a multiscale modeling approach consisting of coarse-grained empirical molecular docking (for binding predictions) and highly refined *ab initio* density functional theory (for the electronic structure calculations) were used in the course of our investigations.

The outline of our paper is as follows: in Section 2, we provide some basic background on the use of quantum dots in biology and discuss some background elements of the problem under consideration. In Section 3, an overview of the multiscale simulation approach is described and a brief description of the various computational methods used to analyze the system. In Section 4, we present our major results followed by detailed discussion and conclusions in Section 5.

2. Quantum dots and biology

In the biological field, quantum dots are rapidly gaining popularity due to several advantages they offer over conventional (usually organic) fluorophores. Recent studies of quantum dots have resulted in the development of new fluorescence immunocytochemical probes [12] typically used to detect antigens in tissues. In contrast to organic fluorophores (dyes) such as rhodamine, GFP, and Fluorescein, CdSe nanocrystals show similar or slightly lower quantum yields at room temperature, but the lower quantum yields are compensated by their larger absorption cross-sections and much reduced photobleaching rates. It was estimated that single ZnS-capped CdSe quantum dots are ~20 times brighter and ~100–200 times more stable than single rhodamine 6G molecules [27]. Some of the drawbacks of organic dyes include sensitivity to environmental pH changes, susceptibility to photobleaching, fixed emission spectra, and limited Stokes shifts (separations between excitation and emission maxima which interfere with the detection of a fluorochrome). Quantum dots on the other hand, apart from their high brightness and photostability, also exhibit narrow emission spectra and an apparent large Stokes shift. Fig. 1, taken from the work of Bruchez et al. [4], illustrates the spectral characteristics of CdSe/CdS/Zns quantum dots in comparison with Fluorescein. The current mode of detecting the antigens which takes from 2 to 6 days can be sped to a few hours using quantum dots [35]. Furthermore, quantum dots can even be tuned to fluoresce at different colors with the same wavelength of excitation. This allows multiple tags to be tracked while using a single light source [4]. The reader is referred to the following representative works (among others) that illustrate the varied biological applications of quantum dots: (i) Oligonucleotides were successfully coupled to molecular beacons, which can then serve as a basis for DNA and RNA assays [1], (ii) quantum dots may be used in detection of behavior of the cells which cause breast cancer [12], (iii) quantum dots can be used in live and fixed fluorescence cell labeling such as cellular tracking, stem cell differentiation tracking, genetic instability monitoring, and molecular location tracking [1], and (iv) quantum dots have been used in the study of antibiotic release into the cell [1].

CdSe quantum dots (the system of interest in the present study) can emit light spanning the entire visible range from blue[1] to red (490–620 nm) depending on size (2–20 nm) [15]. Thus, with tuning of CdSe quantum dot radii, it is possible to realize labels that have emission spectra at several selected wavelengths throughout the visible spectrum. Moreover, electrons in all of these quantum dots may be excited with a light source of one wavelength as long as the wavelength of the source is shorter than that of the emission wavelengths of all of the dots; accordingly, the simultaneous observation of multiple biological structures may be accomplished by labeling them with quantum dots of different colors and by pumping all of these quantum dots with the same source. This is in contrast to the situation encountered for fluorescent dyes, since each dye generally requires an excitation source of a well defined wavelength. Each of these different-colored quantum dots may be functionalized with a unique ligand–biomolecule pair to facilitate binding to a particular biological structure. Fig. 1 illustrates a comparative study on the emissive and excitation properties of CdSe quantum dots and a bio-label called Fluorescein; notice the broad differentiation in the emission and excitation spectrums of the quantum dot as well as the size dependence of its emissive wavelengths [4].

Designing and fabricating semiconductor quantum dots that remain fluorescent in aqueous media and the conjugation of quantum dots with molecules that have affinities for binding to specific biological structures is the major challenge that needs to be addressed in biological use of quantum dots. Quantum dots are usually functionalized by organic compounds such as mercaptoacetic acid [6] or coated with a hydrophilic layer such as silica [12] in order to make them water soluble and biocompatible. One means of functionalizing quantum dots is conjugating CdS quantum dots or ZnS-capped CdSe quantum dots with peptide sequences with certain patterns [6]. Binding to quantum dots in most cases relies on a ligand containing a carboxyl group or an amine group. Cross-linking takes place resulting in the covalent bonding of the carboxyl (or amine) group present in the ligand on the quantum dot to an amine (or carboxyl) group on a biomolecule. Many biomolecules such as proteins, antibodies, and DNA contain carboxyl and amine groups [1]. DNA is a useful linker molecule that acts like molecular glue which can bind the capped quantum dots to bigger biological systems like bacteria. The DNA used in our study was a 12-mer (12-nucleotide linkage) of B-form with around 800 atoms (568 atoms before adding hydrogen atoms to the structure; protein database ID: 1 bna).

3. Overview of the multiscale approach

The prototype model system is comprised of a quantum dot (<2 nm, fewer than 100 atoms) and a DNA molecule (thousands of atoms). The sheer difference in length scales challenge the analytical modeling and numerical simulations. Thus we used a multiscale approach that takes into account the requisite treatment commensurate with each aspect of the interaction. In spite

[1] For interpretation of color in Fig. 1, the reader is referred to the web version of this article.

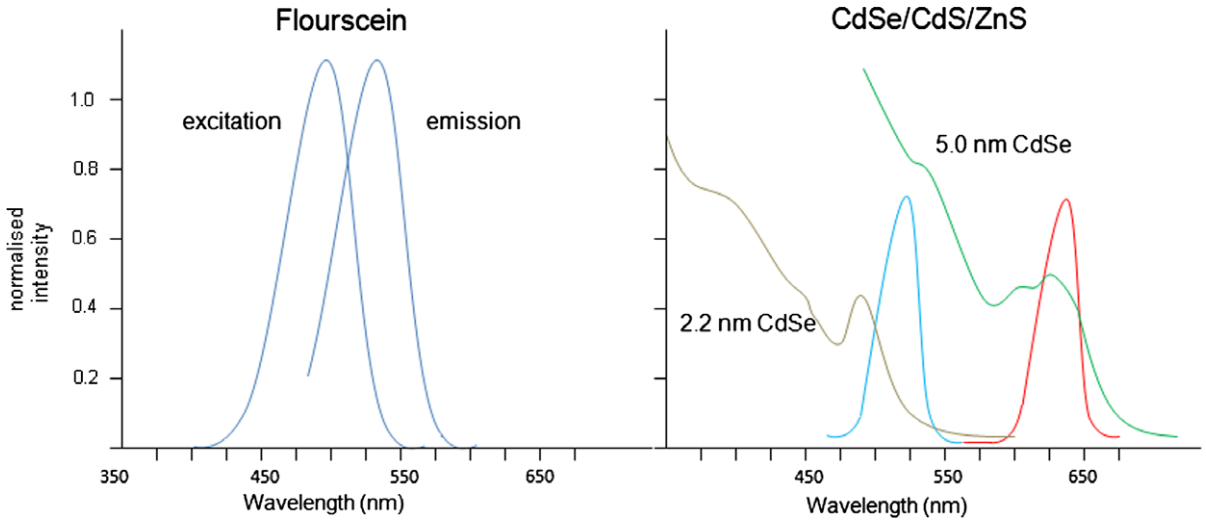

Fig. 1. Comparison between an organic dye (Fluorescein) and a ZnS-capped CdSe quantum dot used in fluorescence labeling (adapted and re-drawn: source: 4).

of using small-sized quantum dots for this work (1.0–1.3 nm), handling the collective number of atoms in the range of a 1000 remained a challenge. While *ab initio* density functional theory fails in handling large system sizes, classical molecular mechanics is problematic due to non-availability of force field parameters for these types of systems (and of course cannot be used to compute the electronic structure for the requisite band gap calculations). Accordingly we have broken down the problem into several stages involving different computational methods. An overview of the computational approach we employed is described below:

(1) *Construction of the quantum dot in sizes* 1.0 *nm,* 1.1 *nm, and* 1.3 *nm*: CdSe is a direct band gap semiconductor and its bulk form exists in two major crystalline lattice structures: wurtzite (hexagonal) and zinc blende (cubic) [23]. Notably, the energy difference between these two forms is small. We have used the zinc blende structure for our simulations. In practice spherical quantum dots are typically synthesized using colloidal processes, which is a controlled precipitation technique, yielding an inorganic semiconductor core coated by chemically adsorbed trioctylphosphine oxide (TOPO) [7]. The TOPO caps the nanocrystals and stabilizes its surface, determines the particle solubility, and prevents an irreversible flocculation or aggregation of the nanocrystals [41]. Accordingly we have chosen the spherical geometry obtained by truncation of the bulk structure. The latter process leads to several dangling bonds.

(2) *Passivation*: For accurate band gap calculations, the dangling bonds of the surface atoms of the quantum dot must be saturated. The passivation is not as trivial as for elemental Silicon due to the valence structure of the CdSe. As alluded to earlier, common capping agents for CdSe quantum dots are ZnS (in a core shell model), mercaptoacetic acid, TOPO and others. Due to the complexity of the nature of these capping agents and lack of chemical models representing them, pseudo-hydrogen atoms were used as passivating atoms. For the CdSe system, a pseudo-hydrogen atom contains a nuclear charge other than 1. A pseudo-potential that represented this 'new' kind of atoms was specifically built for this work.

(3) *Relaxation of the quantum dot structure*: The passivated quantum dots were relaxed using quantum mechanical density functional theory since the size of the system was small (and no reliable empirical potentials are available). The relaxation was followed by an electronic band structure calculation (also using density functional theory) which determines the initial quantum confinement state for the quantum dot (prior to DNA interaction).

(4) *Molecular docking with DNA*: This process ensures identification of the highest probability location of the dot relative to the DNA. The docking algorithm uses electrostatic and Van der Waal interactions to determine the high probability locations. In our calculations we employed the Monte Carlo simulated annealing approach. The macromolecule remains fixed throughout the simulation, and the ligand molecule performs a random walk in the 3D space around it. A small amount of random displacement is applied to each of the degrees of the freedom of the ligand molecule namely translation and rotation of the dihedral bond angles, the number of which is set at the beginning of the docking calculation. This change leads to a new configuration, and therefore a new value of the interaction energy which is calculated using the grid interpolation method. The new energy value is contrasted with the preceding one and if found lower, the new configuration is accepted. In the reverse case, acceptance or rejection is based on a temperature dependent probability expression, where the probability of acceptance is

$$P(\Delta E) = e^{(\Delta E/K_B T)}. \tag{1}$$

Here ΔE is the energy difference from the previous step, and k_B is the Boltzmann constant. When temperatures are high enough, almost all steps are accepted while at lower temperatures, fewer high energy configurations are accepted.

The pair-wise potential energy, $V(r)$, between two non-bonded atoms can be expressed as a function of internuclear separation, r, as follows:

$$\mathbf{V}(r) = \frac{Ae^{-br}}{r} - \frac{c_6}{r_6}. \tag{2}$$

The exponential, repulsive, exchange energy is often approximated with a polynomial form that is computationally more expedient,

$$\frac{Ae^{-br}}{r} = \frac{C_{12}}{r^{12}}. \tag{3}$$

Hence pair-wise-atomic interaction energies can be approximated using the following general equation:

$$\mathbf{V}(r) = \frac{C_n}{r^n} - \frac{C_m}{r^m}, \tag{4}$$

where m and n are integers, and C_n and C_m are constants whose values depend on the depth of the energy well and the equilibrium separation of the two atoms' nuclei. Typically the 12–6 Lennard–Jones parameters ($n = 12$, $m = 6$) are used to model the Van der Waals' forces experienced between two instantaneous dipoles. However, the 12–10 form of this expression ($n = 12$, $m = 10$) can be used to model hydrogen bonds [25].

(5) *Quantum dot–DNA interaction*: The geometrically relaxed quantum dot, at the appropriate favorable docked site is *further relaxed in the presence* of the DNA. We have used density functional theory to obtain the quantum dot–DNA interaction. We used the plane wave self-consistent field (PWscf) method to relax the docked system of quantum dot and the DNA. This method although precise in calculating the ground state total energy and electron density of a system of interacting electrons is limited by the size of the system that it can handle. We therefore truncated the DNA to include only the atoms in the region closest to the quantum dot determined from the docked position between the two members. The DNA molecule was capped at the truncated region with hydrogen atoms.

(6) *Electronic structure calculation of the 'perturbed' quantum dot using DFT*: The band gap of the quantum dot is calculated using DFT to assess the impact of the DNA on its optical signature. DFT is an *ab initio* based technique that is designed to give an approximate result for the ground state energy of a system through a self-consistent calculation. DFT also exhibits well-known limitations in terms of band gap calculations and this aspect will be discussed in due course. We briefly review this method here (as many readers of this journal may be unfamiliar with it). Our discussion is heavily based on a simple tutorial given by Wills and Eriksson [40]. The reader is referred to any number of excellent books available for more details e.g. Martin [24]. The goal of any first principle approach (i.e. based on quantum mechanics requiring no adjustable parameters) is to compute the total minimum quantum mechanical energy of a system with respect to nuclear and electronic coordinates. Due to the many-body nature of the problem, except for some very simple simples, a pragmatic outlook involves making some approximations. DFT provides a simple (and popular) recipe to handle the otherwise draconian computation. The starting point is the total Hamiltonian for an n-electron system:

$$H\psi(\mathbf{r}_1, \mathbf{r}_2, \ldots, \mathbf{r}_n) = E\psi(\mathbf{r}_1, \mathbf{r}_2, \ldots, \mathbf{r}_n). \tag{5}$$

The key concept underlying DFT is that, instead of the many-body wavefunction, the ground state energy may be *uniquely* cast in term of the electronic density. More precisely, the ground state energy is a functional of the electron density and may be estimated by a variational minimization of the functional. Unlike the many-body wavefunction, the electron density is a function of a *single* coordinate. One can replace the ground state energy (which is a function of a the many-body wavefunction in Eq. (5) by

$$n(r) = \sum_{i=1}^{n} \int \psi * (\mathbf{r}_1, \mathbf{r}_2, \ldots, \mathbf{r}_n)\delta(\mathbf{r} - \mathbf{r}_i)\psi(\mathbf{r}_1, \mathbf{r}_2, \ldots, \mathbf{r}_n)\mathrm{d}\mathbf{r}_1, \ldots, \mathrm{d}\mathbf{r}_n. \tag{6}$$

The second concept [17,19] is that one only solves for a single electron state but using an effective potential. The solution should yield the actual many-body density. Mathematically,

$$\begin{aligned} &(\widehat{T} + V_{\mathrm{eff}})\psi_i(\mathbf{r}) = \varepsilon_i\psi_i(\mathbf{r}), \\ &n(\mathbf{r}) = \sum_{i=1} |\psi_i(\mathbf{r})|^2. \end{aligned} \tag{7}$$

$\widehat{T}$ is the quantum mechanical kinetic energy operator. The effective potential is given by

$$V_{\mathrm{eff}}(\mathbf{r}) = \frac{\delta}{\delta n(\mathbf{r})}\{E_H[n(\mathbf{r})] + E_{\mathrm{xc}}[n(\mathbf{r})] + E_{\mathrm{eN}}[n(\mathbf{r})]\}. \tag{8}$$

The various components of the effective potential, the Hartree term (E_{H}), electron–nuclei interaction E_{eN} and the exchange-correlation term E_{xc} are obtained from the total energy functional which also involves the kinetic energy and the nuclei–nuclei repulsion:

$$E[n(\mathbf{r})] = T[n(\mathbf{r})] + E_H[n(\mathbf{r})] + E_{\mathrm{xc}}[n(\mathbf{r})] + E_{\mathrm{eN}}[n(\mathbf{r})] + E_{\mathrm{NN}}, \tag{9}$$

where

$$\begin{aligned} T[n(\mathbf{r})] &= \sum_i \int \psi_i^* \widehat{T}\psi_i \,\mathrm{d}\mathbf{r}, \\ E_H[n(\mathbf{r})] &= \frac{e^2}{2}\int \frac{n(\mathbf{r}_1)n(\mathbf{r}_1)}{|\mathbf{r}_1 - \mathbf{r}_2|}\,\mathrm{d}\mathbf{r}_1\,\mathrm{d}\mathbf{r}_1, \\ E_{\mathrm{eN}}[n(\mathbf{r})] &= -e^2\sum_R Z_R \int \frac{n(\mathbf{r})}{|\mathbf{r} - \boldsymbol{R}|}\,\mathrm{d}\mathbf{r}, \\ E_{\mathrm{NN}} &= \frac{e^2}{2}\sum_R \sum_{R' \neq R} \frac{Z_R Z_{R'}}{|\boldsymbol{R}' - \boldsymbol{R}|}, \\ E_{\mathrm{xc}}[n(\mathbf{r})] &= \int n(\mathbf{r})\varepsilon_{\mathrm{xc}}[n(\mathbf{r})]\mathrm{d}\mathbf{r}. \end{aligned} \tag{10}$$

The last term involves the exchange-correlation functional (under the integral sign) and the expression is in the so-called local density approximation. The accuracy of the DFT scheme relies on a faithful evaluation of this term. Usually, values for this are established via quantum Monte Carlo techniques. These equations are solved self-consistently to converge to the desired ground state energy. In practice, the single particle equations are solved by expanding the wavefunction into a suitable set of basis functions. In our calculations, we have used the plane-wave expansion.

The relaxation of nanostructures based on density functional theory calculates the forces acting on each atom as

$$\mathbf{F}_i = -\frac{\mathrm{d}E}{\mathrm{d}\mathbf{R}_i}, \tag{11}$$

where E is the total energy of the atoms and $\mathbf{R}_i$ is the position vector of the ith atom. The atoms' positions are changed based on the optimization algorithm BFGS (Broyden–Fletcher–Goldfarb–Shanno).

4. Computational details

In this section, we provide some of the computational details of our approach described in the preceding section.

4.1. Construction and passivation

The need for passivation arises due to the presence of unsaturated surface bonds or dangling bond states. These electronically active states have to be quenched by re-bonding with a passivation agent to establish neutrality of the system. A good surface passivation will remove the localized surface states from the band gap, but will not change the intrinsic nature of the highest energy occupied molecular orbital (HOMO) and the lowest energy unoccupied molecular orbital (LUMO) which characterize the electronic structure of each material. For group IV semiconductors, hydrogen is often used as a passivating agent. This choice is quite expedient as the electronegativity of the hydrogen atom is comparable to that of Si and Ge and the H–Si or H–Ge bond provides a convenient structural and electronic termination of the nanostructure [18]. For II–VI type semiconductors, experimentally, organic molecules like trioctylphosphine (TOP) or trioctylphosphine oxide (TOPO) are often used to passivate nanoparticles [32]. However, these passivation agents have a complex chemistry and a thorough under-

standing of their atomic nature in computational work is still inadequate.

Some of the previous work involving passivation of semiconductor nanoparticles includes Wang and Zunger [39] who proposed an empirical "ligand potential" for quantum dots of CdSe. In this model, by placing positive (negative) short ranged electrostatic potentials near surface cations (anions) and choosing a Gaussian form of the ligand potential with parameters chosen based on the surface electron states, they were able to create a simple atomistic model. However, some shortcomings in this approach, especially in the case of non-stoichiometric CdSe quantum dots are that, this procedure does not completely remove some of the gap states and an artificial shift of the Fermi level is required [33]. Also it is not clear whether a single ligand potential could be used for a variety of dangling bonds and due to the empirical nature of the parameterization no criteria exists to optimize the passivation procedure. Shiraishi [34] proposed a new slab model approach for a GaAs surface. They fashioned fictitious hydrogen atoms, H^* to passivate the surface. Their fictitious hydrogen potentials were based on fractionally charged hydrogen atoms, i.e., a fractional proton charge with a corresponding fractional electron charge. The choice of the fractional proton charge is based on a simple chemical consideration of a covalent bond. In GaAs, the formal valence of Ga is three and As is five. As such, 3/4 of an electron from each Ga atom and 5/4 of an electron from each As atom combine and form covalent bonds between them. Therefore, the fractional 3/4 (5/4) charged fictitious atoms are considered as an appropriate choice to terminate the surface As (Ga) dangling bonds. Wang and Li proposed a similar model where they used fictional hydrogen-like atoms to passivate III–V and II–VI semiconductor quantum dots [21]. In their work, they used a nuclear charge of (8-m)/4 to passivate a surface atom with formal valence charge 'm'. Huang et al. [18] used a similar system for surface passivation. He proposed a quantitative norm for choosing the passivating potentials which was based on a 'metric' found through an analysis of group IV semiconductors. He used density-functional theory within the local-density approximation to solve for the electronic structure of GaAs quantum dots and *ab initio* pseudo-potentials were generated using the Troullier–Martins prescription [36]. There are no repercussions of choosing this fictitious passivation ligand. It is a well tested methodology as seen above [18,21]. The key benefit of the assumption is ease in modeling and reduced computational load. Band gap energy values arrived from experimental and computational means using "real life" ligands and pseudo-hydrogen atoms, respectively, have shown close correlation [18].

For the case of hydrogen passivated Si surfaces $Z = 1$, however for III–V and II–VI systems, Z is not an integer. From the literature, $Z = 1.0, 0.75, 0.5, 1.25, 1.5$ for IV, V, VI, III, II row atoms, respectively [38]. A half bulk bond length is used as the H^* atom to surface atom bond length for all the systems. Accordingly, two kinds of pseudo-hydrogen atoms are used in our modeling tool[2]: one for capping cadmium and the other one for capping selenium. Thereby, we have the cadmium: pseudo-hydrogen with $Z = 1.5$ nuclear charge and the selenium: pseudo-hydrogen is $Z = 0.5$ nuclear charge. The pseudo-potentials for the aforementioned pseudo-hydrogen atoms were generated using Vanderbilt's ultrasoft pseudo-potential generation package (USPP-7.3.6) [37]. The standard method for generation of the pseudo-potential for the hydrogen atom was modified to account for a partial nuclear charge and the appropriate semicore shells were included in valence. The exchange-correlation used by the program was Ceperley–Alder [5] in Perdew–Zunger parameterization [29].

To obtain the equilibrium bond length of cadmium and selenium atoms with the pseudo-hydrogen atoms, a simple relaxation involving a tetrahedral structure, shown in Fig. 2 with one cadmium atom and four pseudo-hydrogen atoms was performed using DFT with the ultrasoft pseudo-potential for cadmium and the newly generated pseudo-potential for pseudo-hydrogen atoms. A similar procedure is adopted for the selenium atoms as well. The cadmium–X (pseudo-hydrogen) bond length was found to be 1.798 Å and the selenium–Xa (pseudo-hydrogen) bond length was found to be 1.586 Å. The exact numbers of capping hydrogen atoms are carefully added on the surface to passivate all the dangling bonds. Four CdSe structures of varying size were used for this study: a 1.0 nm, a 1.1 nm, a 1.3 nm and a 1.4 nm (after capping with pseudo-hydrogen atoms) as shown in Fig. 3.

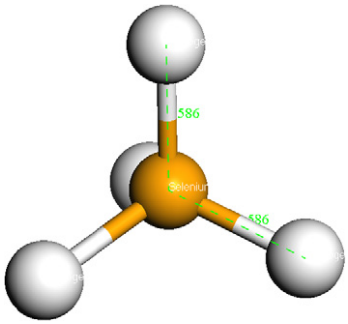

Fig. 2. Single selenium atom bonded to four pseudo-hydrogens and the optimized bond length of 1.586 Å after DFT relaxation.

4.2. Relaxation of the quantum dot structure

DFT was used to perform the relaxation of the quantum dot.[3] A simple cubic lattice is assumed with lattice parameter $a = 3.0$ (in Bohr), 26 atoms in the unit cell with four species of atoms. The kinetic energy cutoff (Ry) for the wave function was taken as 25 with the maximum number of iterations in a self-consistent field step (SCF) set to 1000. In the SCF method, an initial set of orbitals is used to generate a new set of orbitals and the procedure is repeated until the convergence criteria are met, that is, the energy difference between two sequential steps is less than 10^{-6} Ry. A second order formula is used to extrapolate the wave functions and potential from preceding steps. We have used Vanderbilt's ultra soft pseudo-potentials [37] available for cadmium and selenium [20] from the PWscf library along with generated pseudo-potentials for X and Xa species.

A similar relaxation and band gap study was also repeated on a 1.0 nm quantum dot. The computational results exhibited absence of HOMO–LUMO differentiation with several energy states clearly indicating the need for passivation. The reported self-healing of uncapped quantum dot [30] may need re-examination. Some of the relevant results, both before and after relaxation of the quantum dots, are specified in Table 1 and Fig. 4.

4.3. Molecular docking with DNA

Molecular docking must be performed to obtain reasonably favorable "binding" locations between the appropriately relaxed quantum dot and the DNA as a starting position for the actual interaction calculations.[4] The macromolecule (DNA, PDB ID from the nucleic acid database 1bna) and the ligand (quantum dot representation) are individually prepared before docking. Gasteiger charges [13] are computed for the DNA structure. Here, the DNA is

[2] Materials studio 4.1 (Accelrys Inc., 2006).

[3] Using PWscf software [3].

[4] The program used is Autodock 3.0 [25].

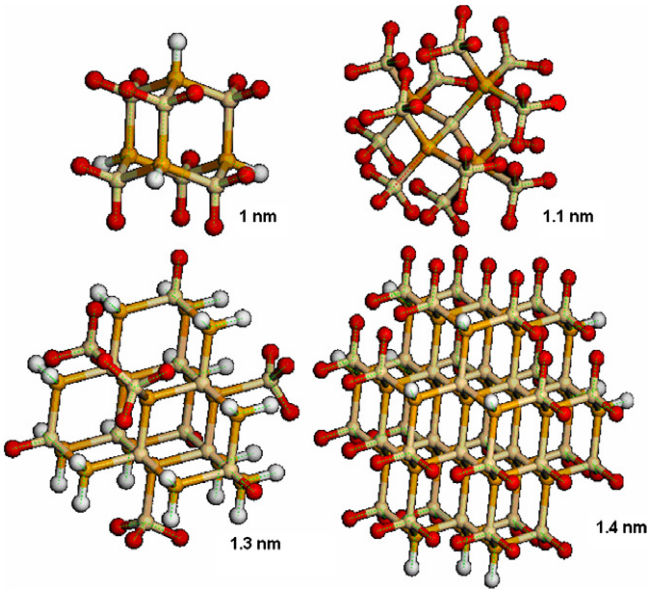

Fig. 3. The above models show capped CdSe quantum dots of various diameters: cadmium: (orange); selenium: (beige); X hydrogen: (red); Xa hydrogen: (white). (a) 1 nm, (b) 1.1 nm, (c) 1.3 nm, and (d) 1.4 nm. (For interpretation of the references in color in this figure legend, the reader is referred to the web version of this article.)

fixed and the quantum dot is given a set of torsions, in our case 16, for the 1.1 nm quantum dot to provide degrees of freedom for it to relax in the presence of the DNA. Torsions help in the definition of rotatable bonds in small molecules. Partial atomic charges are used to compute the electrostatic interaction energy using Coulomb's law and also for a qualitative understanding of the structure and reactivity of molecules. Partial charges for ligand atoms have been computed earlier by different methods. [10] used first principle methods on bulk CdSe; more recently [32] used semi empirical methods to determine partial charges; in the present work, we have calculated the partial charges of all the atoms in the system as Lowdin charges [22] using DFT after relaxing the quantum dot.[5] This method determines atomic populations from projecting the electron density onto the nuclei. The partial charge for the three atom types (Cd, Se, and capping atoms) were different depending on what atom each of them were bonded to. Hence it was important to calculate them from first principles rather than assume a charge based on their electronegativities. Cadmium has a positive charge between 1.839 and 1.675; selenium has a negative charge between −1.820 and 1.821 and capping atom (pseudo-hydrogen) has a net negative charge between −0.424 and −0.428.

The computational grid is set up as a rectangular box encompassing the DNA. Since there is no *a priori* information on where the quantum dot would prefer to reside relative to the DNA the whole molecule is used for the search algorithm (Lamarckian genetic algorithm). This is computationally intensive but removes any bias on the search for the preferred locations. The interaction between the macromolecule and ligand is heavily dependent on type of atoms, the number of atoms, and partial charges and the position of these atoms. A set of 10 calculations (total sample size of 200) were run on the 1.1 nm sized dot to generate enough statistical data. After checking the set of locations determined by the docking procedure relative to the DNA, one suitable location is chosen based on the lowest interaction energy.

The searched set of coordinates of the DNA and the quantum dot, form a starting point for our next level of calculations. In Fig. 5, we show one such configuration of the two molecules with respect to each other.[6]

4.4. Quantum dot–DNA interaction: combined relaxation using DFT

Ideally, the next phase of this calculation would be the *combined* relaxation of the configuration(s) determined from the docking calculation. This is an especially important step because the DNA molecule was fixed during the docking calculations and there was no feed-back mechanism for the DNA to relax in the presence of the QD or for the QD to respond to any changes in the DNA. Also, the DNA configuration was not obtained from a co-crystal but from an un-bounded solution-phase free DNA duplex. However, as mentioned earlier, this is not possible due to the unavailability of suitable empirical force fields. The latter remains one of the major impediments in large scale high fidelity computation of this problem. Accordingly, in the present work, we have used DFT once again to assess the interactions of the combined system. While certainly this approach is expected to be more accurate than empirical force field computation, the major drawback is its inability to handle large numbers of atoms and, as such, we could only use a portion of the DNA molecule in the interaction studies in addition to small-sized quantum dots (1.1 and 1.3 nm).

5. Results and discussion

The quantum dot HOMO–LUMO energy gaps before and after interactions with the DNA are reported in Table 2. As is well-known, DFT is suitable for ground state total energy calculations and, for example, underestimates energy gaps. Remedies exist to correct this (e.g. [16,43,31,8]). Here, we employed a constant additive factor to correct for this based on the bulk band gap values [9]. In any event, our interests are in relative shifts which are expected to be reasonable.

Evidently, we do not observe a *significant change* in the energy gap. We observe a small (albeit measurable) 'red shift'. We cannot at this point draw parallels between previously reported experimental results and our computational work nor can we conclusively explain the exact reason for the large wavelength shift seen in the experiment. However, we can draw some preliminary conclusions. The maximum quantum dot diameter that we have so far simulated is 1.3 nm without the ZnS and the bio-polymeric layers of coating used in the commercially available quantum dots (core diameters 4–10 nm). Given that with increasing size, based on the qualitative trends from our work as well as on physical grounds, we expect the shift to be even smaller; the contrast between our results and the singular experimental evidence is puzzling and requires re-examination. Furthermore, we note here that our simulations are carried out in vacuum (corresponding to the vacuum dielectric constant). In realistic scenarios, screening effect of the embedding fluid will further serve to *decrease the shift yet further* thus effectively ruling out the role of non-bonded interactions in the use of quantum dots as biosensors. We speculate that in absence of active engineering of either the quantum dot surface or through other means (perhaps through defects), quantum dot interaction with biomolecules is likely to be small leaving FRET (fluorescence resonance energy transfer) as the dominant current interaction mechanism. This assertion is supported by at least one empirical work [28]. These authors attempted to employ CdSe quantum dots to detect trace amounts of 2, 4, 6 trinitrotoluene. The shifts observed by them are also around 8–12 nm. Once

[5] The program used is PWscf [3].

[6] The images are rendered with VMD software support (The Theoretical and Computational Biophysics group at the Beckman Institute, University of Illinois at Urbana-Champaign) [26].

Table 1
HOMO–LUMO and band gap energy values before and after relaxation

	1 nm		1.1 nm		1.3 nm		1.4 nm	
	Before	After	Before	After	Before	After	Before	After
HOMO (eV)	−6.95	−7.08	−6.90	−7.25	−5.82	−5.88	−5.64	−5.80
LUMO (eV)	−2.27	−2.42	−3.22	−3.19	−2.35	−2.39	−2.77	−2.84
Band gap (eV)	−4.65	−4.68	−3.67	−4.06	−3.46	−3.49	−2.88	−2.96

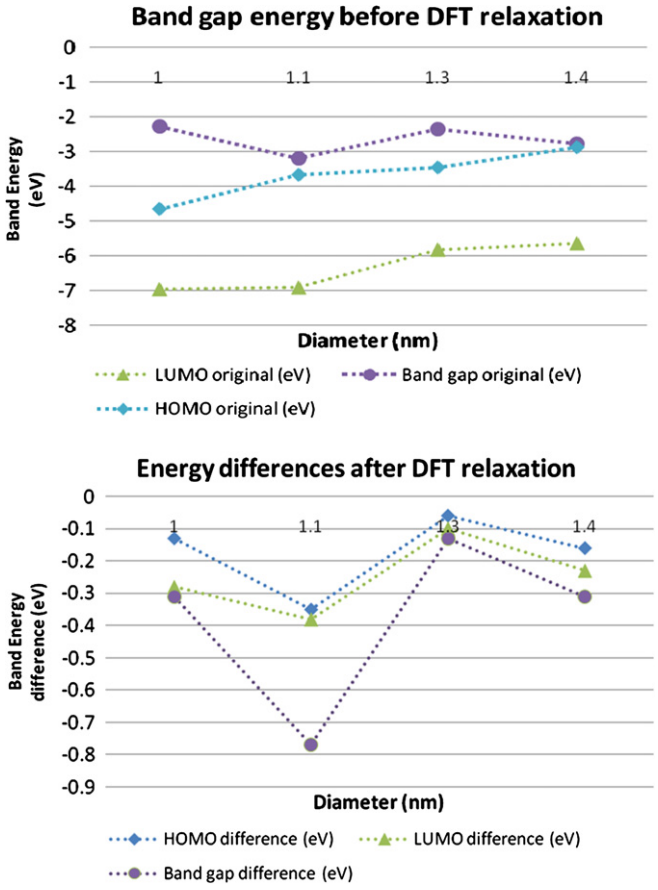

Fig. 4. HOMO–LUMO levels and bandgap before and after relaxation of 1.0 nm, 1.1 nm, 1.3 nm and 1.4 nm quantum dots.

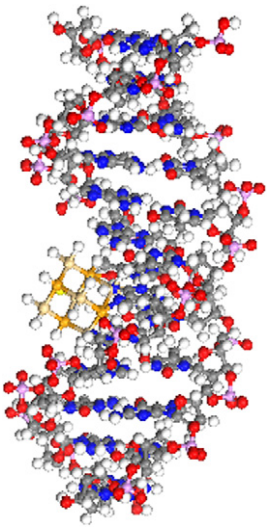

Fig. 5. The docked position of the quantum dot and the DNA.

Table 2
Band gap and wavelength shifts before and after interaction with DNA for 1.1 nm and 1.3 nm quantum dots

	Original	After final interaction with DNA	Final shift
Size = 1.1 nm			
Bandgap (eV)	4.0591	3.8199	0.2392
Wavelength (nm)	306	325	19
Size = 1.3 nm			
Bandgap (eV)	3.4928	3.3799	0.1120
Wavelength (nm)	356	368	12

source of error in our computation requires further work namely, the DNA and QD are not co-relaxed and only the QD is relaxed in the *presence* of the DNA. In reality, the changes in QD are expected to impact the DNA configuration as well. We speculate that this error is small however, in absence of any rigorous proof, this assumption is best revisited in the future.

References

[1] D. Alexson, H. Chen, M. Cho, M. Dutta, Y. Li, P. Shi, A. Raichura, D. Ramadurai, J. Phys.: Condens. Mat. 17 (2005) R637–R656.
[2] A. Alivisatos, Nature 430 (6996) (2004) 190–195. ISSN: 0028-0836.
[3] S. Baroni, A. Dal Corso, S. de Gironcoli, P. Giannozzi, 1999. <http://www.pwscf.org>.
[4] M. Bruchez, M. Moronne, P. Gin, S. Weiss, A.A. Alivisatos, Science 281 (1998) 2013–2016.
[5] D.M. Ceperley, B.J. Alder, Phys. Rev. Lett. 45 (1980) 566.
[6] W. Chan, S. Nie, Quantum dots bioconjugates for ultrasensitive nonisotopic detection, Science 281 (5385) (1998) 2016–2018.
[7] W. Chan, D. Maxwell, X. Gao, R. Bailey, M. Han, S. Nie, Curr. Opin. Biotechnol. 13 (2002) 40–46.
[8] E. Degoli, G. Cantele, E. Luppi, R. Magri, D. Ninno, O. Bisi, S. Ossicini, Phys. Rev. B 69 (2004) 155411.
[9] B. Delley, E.F. Steigmeier, Phys. Rev. B 47 (1993) 1397.
[10] Y. Duan, M. Jungen, Eur. Phys. J. B 2 (1998) 183.
[11] S. Dwarakanath, J. Bruno, A. Shastry, T. Phillips, A. John, A. John, A. Kumar, L. Stephenson, Biochem. Biophys. Res. Commun. 325 (3) (2004) 739–743. 15541352.
[12] H. Gao, K. Yong, Annu. Rev. Mater. Res. 34 (2004) 123–150.
[13] J. Gasteiger, M. Marsili, Tetrahedron 36 (1980) 3219.
[14] D. Geho, Nicholas Lahar, Prem Gurnani, Michael Huebschman, Paul Herrmann, Virginia Espina, Alice Shi, Julia Wulfkuhle, Harold Garner, Emanuel Petricoin, Lance A. Liotta, Kevin P. Rosenblatt, Bioconjugate Chem. 16 (2005) 559–566.
[15] Harnessing the power of quantum dots, Quantum dots explained web site, 2005. <http://www.evidenttech.com/quantumdot-definition/quantum-dot-use.php>.
[16] L. Hedin, Phys. Rev. 139 (1965) A796.
[17] P. Hohenberg, W. Kohn, Phys. Rev. 136 (1964) 864.
[18] X. Huang, E. Lindgren, J. Chelikowsky, Phys. Rev. B (Condens. Mat. Mater. Phys.) 71 (16) (2005) 165328-1–165328-6.
[19] W. Kohn, L.J. Sham, Phys. Rev. 140 (1965) A1133–A1138.
[20] K. Kwak, R.D. King-Smith, David D. Vanderbilt, Phys. Rev. B 48 (1993) 17827–17834.
[21] J. Li, Lin-Wang Wang, Appl. Phys. Lett. 84 (18, 3) (2004) 3648–3650.
[22] P. Lowdin, P. Mukherjee, Chem. Phys. Lett. 14 (1972) 1.
[23] O. Madelung, U. Rössler, M. Schulz, (Eds.), Landolt Börnstein Numerical Data and Functional Relationship in Science and Technology, in: New Series vol. 41B: II-VI and I-VII Compounds; Semimagnetic Compounds, Springer-Verlag, Berlin, 1999.
[24] R.M. Martin, Electronic Structure: Basic Theory and Practical Methods, Cambridge Press, 2004.
[25] G. Morris, G. Goodsell, D. Halliday, R. Huey, R. Hart, W. Belew, A. Olson, J. Comput. Chem. 19 (1998) 1639–1662.
[26] M. Nelson, W. Humphrey, F. Gursoy, A. Dalke, L. Kale, R. Skeel, K. Schulten, NAMD-A parallel, object-oriented molecular dynamics program, Internat. J. Super. Appl. High Perform. Comput. 10 (4).

[27] S. Nie, Warren, Science 281 (5385) (1998) 2016–2018. ISSN: 0036-8075.
[28] S. Nietoa et al., Sensors and command, control, communications and intelligence (C3I) technologies for homeland security and homeland defense III, in: E.M. Carapezza (Ed.), Proc. of SPIE, vol. 5403, SPIE, Bellingham, WA, 2004.
[29] J.P. Perdew, A. Zunger, Phys. Rev. B. 23 (1981) 5048.
[30] A. Puzder, A. Williamson, F. Gygi, G. Galli, Phys. Rev. Lett. 9221 (2004) 217401/1–217401/4.
[31] A. Puzder, A.J. Williamson, J.C. Grossman, G. Galli, J. Am. Chem. Soc. 125 (2003) 2786.
[32] E. Rabani, J. Chem. Phys. 115 (3, 15) (2001) 1493–1497.
[33] E. Rabani, B. Hetenyi, B.J. Berne, L.E. Brus, J. Chem. Phys. 110 (1999) 5355.
[34] K. Shiraishi, J. Phys. Soc. Jpn. 59 (1990) 3455.
[35] A. Smith, X. Gao, S. Nie, Photochem. Photobiol. 80 (3) (2004) 377–385.
[36] N. Troullier, J.L. Martins, Phys. Rev. B 43 (1991) 1993.
[37] D. Vanderbilt, Phys. Rev. B (Rapid Commun.) 41 (1990) 7892.
[38] L. Wang, J. Li, Phys. Rev. B (Condens. Mat. Mater. Phys.) 69 (15) (2004) 153302-1–153302-4.
[39] L. Wang, A. Zunger, Phys. Rev. B 53 (1996) 9579–9582.
[40] J.M. Wills, O. Eriksson, Los Alamos Sci. (26) (2000) 128.
[41] S. Yun, G. Lee, J. Kim, S. Shin, Solid State Commun. 137 (6) (2006) 332–337.
[42] P. Zhang, J. Fluoresc. 16 (3) (2006).
[43] A. Zunger, Phys. Status Solidi B 224 (2001) 727.